

# ESR study of the spin ladder with uniform Dzyaloshinskii-Moria interaction.

V.N. Glazkov,<sup>1,2,\*</sup> M. Fayzullin,<sup>3</sup> Yu. Krasnikova,<sup>4,2</sup> G. Skoblin,<sup>4,2,†</sup> D.Schmidiger,<sup>5</sup> S.Mühlbauer,<sup>5,‡</sup> and A.Zheludev<sup>5</sup>

<sup>1</sup>*P.L.Kapitza Institute for Physical Problems RAS, Kosygin str. 2, 119334 Moscow, Russia*

<sup>2</sup>*Moscow Institute of Physics and Technology, 141700 Dolgoprudny, Russia*

<sup>3</sup>*Institute for Physics, Kazan Federal University, 18 Kremlyovskaya str. 18, 420008, Kazan, Russia*

<sup>4</sup>*Kapitza Institute for Physical Problems RAS, Kosygin str. 2, 119334 Moscow, Russia*

<sup>5</sup>*Neutron Scattering and Magnetism, Laboratory for Solid State Physics, ETH Zürich, 8006 Zürich, Switzerland*

(Dated: September 29, 2018)

Evolution of the ESR absorption in a strong-leg spin ladder magnet  $(\text{C}_7\text{H}_{10}\text{N}_2)_2\text{CuBr}_4$  (abbreviated as DIMPY) is studied from 300 K to 400 mK. Temperature dependence of the ESR relaxation follows a staircase of crossovers between different relaxation regimes. We argue that the main mechanism of ESR line broadening in DIMPY is uniform Dzyaloshinskii-Moria interaction ( $|\mathbf{D}| = 0.20$  K) with an effective longitudinal component along an exchange bond of Cu ions within the legs resulting from the low crystal symmetry of DIMPY and nontrivial orbital ordering. The same Dzyaloshinskii-Moriya interaction results in the lifting of the triplet excitation degeneracy, revealed through the weak splitting of the ESR absorption at low temperatures.

PACS numbers: 75.10.Kt, 76.30.-v  
Keywords: low-dimensional magnet

## I. INTRODUCTION.

Low-dimensional magnets are actively studied during last decades both theoretically and experimentally. Spin-ladder is one of the simplest models of the field, that is just one step more complicated than the Heisenberg spin chain, the keystone of the low-dimensional magnetism. Such a system consists of two chains forming the "legs" of the spin ladder, which are coupled by simple interchain coupling forming "rungs" of the ladder. The Hamiltonian of the single spin ladder with the equivalent positions along the ladder is

$$\mathcal{H} = J_{leg} \sum_i (\mathbf{S}_{1,i} \mathbf{S}_{1,i+1} + \mathbf{S}_{2,i} \mathbf{S}_{2,i+1}) + J_{rung} \sum_i \mathbf{S}_{1,i} \mathbf{S}_{2,i} + \mu_B \mathbf{H} \hat{g} \mathbf{S} + \mathcal{H}_{anis} \quad (1)$$

it includes Heisenberg exchange couplings  $J_{leg}$  and  $J_{rung}$ , Zeeman interaction (with usually anisotropic  $g$ -tensor) and weak anisotropic spin-spin interactions  $\mathcal{H}_{anis}$ .

Independently on the ratio between the  $J_{leg}$  and  $J_{rung}$ , the excitation spectrum of the spin ladder is gapped, ground state is non-magnetic and excited states are  $S = 1$  quasiparticles.<sup>1</sup> However, most of the experimentally available examples of the spin ladder systems are the so-called strong-rung ladders with the dominating in-rung interaction  $J_{rung}$ . Strong-leg ladders remains a rarity in this family. Additional complication of the real systems is a presence of the anisotropic spin-spin interactions breaking the ideal symmetry of the Heisenberg model. Such interactions limit excitations lifetime (to the point of total damping in some extreme cases<sup>2</sup>) and could lift degeneracy of the  $S = 1$  states. Thus, estimation of such interactions strength and, ideally, search for the systems with negligible anisotropic part of the

Hamiltonian is an important quest when comparing real magnets with model predictions.

Adequate accounting for the effect of anisotropic interactions in a spin-gap magnet is also a challenge. This problem was addressed in a 1D field theory models via bosonic<sup>3</sup> and fermionic<sup>4</sup> approaches and in an independently developed macroscopic model.<sup>5</sup> However reliable microscopic models remains a rarity (see, e.g. Ref. 6): most of the real spin-gap magnets have a complicated network of the exchange couplings allowing far too numerous possibilities of the anisotropic interactions parameters. The adequate microscopic approaches are of particular interest in connection with a particular case of the effect of a uniform Dzyaloshinskii-Moria interaction on the properties of a quantum magnet.<sup>7</sup>

Recently found organometallic compound  $(\text{C}_7\text{H}_{10}\text{N}_2)_2\text{CuBr}_4$ , abbreviated DIMPY for short, is an example of the strong-leg ladder with very weak anisotropic interactions.<sup>8-11</sup> Presence of the energy gap in the excitation spectrum was revealed by magnetic susceptibility<sup>8</sup>, specific heat<sup>9</sup> and magnetization<sup>11,12</sup> bulk measurements as well as by inelastic neutron scattering.<sup>9,10</sup> The energy gap was found<sup>9</sup> to be 0.33 meV, it can be closed by the magnetic field  $\mu_0 H_{c1} = 3.0$  T, while the saturation field is much higher<sup>12</sup>  $\mu_0 H_{sat} \approx 30$  T. The values of the exchange constants were determined from the DMRG fit of the measured inelastic neutron scattering spectra<sup>11</sup> and were found to be  $J_{leg} = 1.42$  meV and  $J_{rung} = 0.82$  meV. The magnetic field induced ordering is observed at very low temperatures ( $T_N^{(max)} \approx 300$  mK at  $\mu_0 H \sim 15$  T).<sup>11</sup>

Electron spin resonance (ESR) spectroscopy is a powerful tool to probe for the weak anisotropic interactions in the magnetic systems. Inelastic neutron scattering experiments<sup>10</sup> have shown that DIMPY is an almost per-

fect realisation of the Heisenberg spin ladder. ESR technique allows much higher energy resolution (routinely resolved ESR linewidth of 100 Oe corresponds approximately to the energy resolution of  $1 \mu\text{eV}$ ) and thus allows to probe possible effects of anisotropic interactions with high accuracy.

In the present manuscript we report results of the ESR study of low-energy spin dynamics in DIMPY in the temperature range from 400 mK to 300 K. We observe angular and temperature dependences of the ESR linewidth at high temperatures which can be described as an effect of the uniform Dzyaloshinskii-Moria (DM) interaction, which is allowed by the lattice symmetry. At low temperatures we observe splitting of the ESR absorption line due to lifting of the triplet state degeneracy, which is also possibly due to the same DM interaction. Additionally we observe well resolved ESR absorption lines from the inequivalent ladders which allowed an upper estimate of interladder exchange interaction.

## II. SAMPLES AND EXPERIMENTAL DETAILS.

Single crystals of non-deuterated DIMPY were grown from the solution by slow diffusion in a temperature gradient. Samples quality was checked by X-ray diffraction and magnetization measurements. Concentration of the paramagnetic defects estimated from the 500 mK magnetization curve is below 0.05%.

DIMPY belongs to the monoclinic space group  $P2(1)/n$  with lattice parameters  $a = 7.504 \text{ \AA}$ ,  $b = 31.613 \text{ \AA}$ ,  $c = 8.206 \text{ \AA}$  and the angle  $\beta = 98.972^\circ$ .<sup>8</sup> As-grown crystals have a well developed plane orthogonal to the  $b$ -axis and are elongated along the  $a$  direction.

ESR experiments were performed using set of the home-made transmission-type ESR spectrometers at the frequencies 18-38 GHz. Lowest available temperature of 400 mK was obtained by He-3 vapours pumping cryostat. At the measurements below 77 K magnetic field was created by compact superconducting magnets, typical nonuniformity of the magnetic field at the resonance conditions in our experiments is estimated as  $< 5 \dots 20$  Oe depending on the magnet used. High-temperature experiments were done with a resistive water-cooled magnet with the field nonuniformity about 5 Oe.

## III. LATTICE SYMMETRY AND POSSIBLE ANISOTROPIC INTERACTIONS.

Monoclinic unit cell of DIMPY includes four magnetic  $\text{Cu}^{2+}$  ions that belongs to two spin ladders: two pairs of copper ions form rungs of the spin-ladders, which are then reproduced by translations along the  $a$ -axis. This results in the formation of two ladders differently oriented with respect to the crystal<sup>10</sup> (see Figure 1).

Space symmetry of the DIMPY lattice includes inversion center in the middle of each rung and a second order

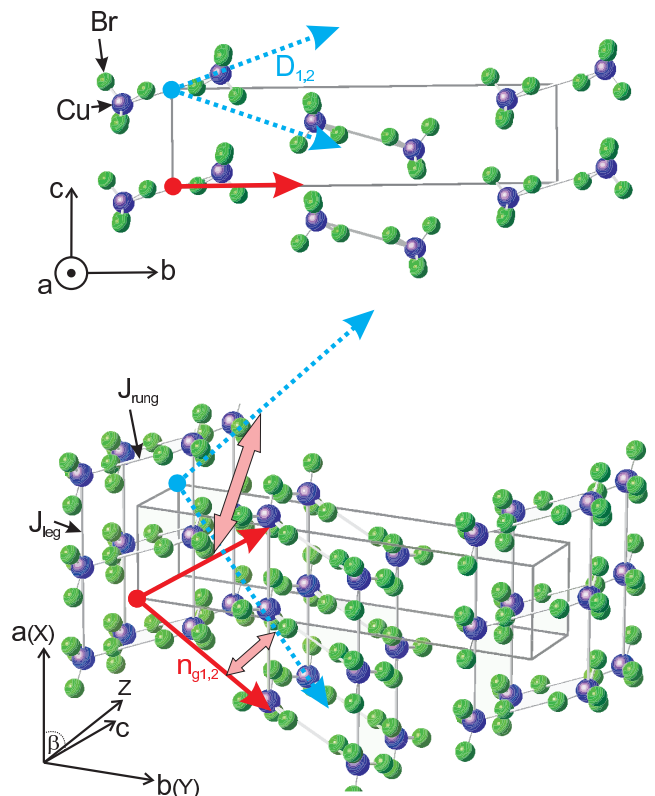


FIG. 1. (color online) Crystallographic structure of DIMPY with two magnetically nonequivalent spin ladders. Only Cu and Br ions are shown along with the main exchange bonds  $J_{leg}$  and  $J_{rung}$ . Solid arrows (red) indicate directions of  $g$ -tensor main axes for inequivalent ladders, dashed arrows (blue) indicate directions of the Dzyaloshinskii-Moriya vectors for inequivalent ladders, as found from the data fit (see text). Broad double-headed arrows links DM vector and  $g$ -tensor axis corresponding to the same ladder.

screw axis parallel to the crystallographic  $b$  direction that links different ladders.

These symmetries place strong restrictions on the possible microscopic anisotropic interactions in DIMPY despite the low crystallographic symmetry. First, all anisotropic interactions along the legs of the ladders should be uniform because of translational symmetry. Second, Dzyaloshinskii-Moria antisymmetric interaction  $\mathcal{H}_{DM} = \mathbf{D} \cdot [\mathbf{S}_1 \times \mathbf{S}_2]$  on the rungs is forbidden by the inversion symmetry. The same inversion symmetry requires that direction of the Dzyaloshinskii-Moria vector  $\mathbf{D}$  have to be exactly opposite on the legs of the same ladder. Third, inversion center on the rungs of the ladder ensures that  $g$ -tensor is always the same for the given spin ladder so there are no complications of anisotropic Zeeman splitting.

Second order axis establish relations between the  $g$ -tensor components and Dzyaloshinskii-Moria vector direction in different ladders. In particular, because of this second order axis the effective  $g$ -factor values are

the same for both ladders for the field applied parallel or orthogonally to this axis.

This analysis neglects anisotropic interladder couplings and possible symmetric anisotropic exchange (SAE) coupling  $\mathcal{H}_{SAE} = \sum_{\mu,\tau} J_{\mu\tau} S_1^\mu S_2^\tau$ , where  $J_{\mu\tau}$  are components of a symmetric exchange tensor  $\hat{\mathbf{A}}$ , which is usually constrained by condition  $Tr J_{\mu,\tau} = 0$ . Symmetric interaction is allowed both on rungs and legs of the ladder and is also constrained by symmetry operations. However, as we will demonstrate below, our observations point that Dzyaloshinskii-Moria interaction is dominating anisotropic interaction in the case of DIMPY.

As for the anisotropic interladder couplings, there is a possibility that anisotropic couplings between the equivalent ladders stacked in  $c$  direction could be important as well: Cu-Cu distance in this direction is even less than the distance on the rungs (8.2 Å against 8.9 Å) and suppression of the Heisenberg exchange interaction in this direction is most likely due to unfavorable mutual orientation of the electron orbitals of bromine ions mediating this superexchange route which could be less important for the anisotropic spin-spin interactions arising through involvement of differently oriented excited electron orbitals mixed with the ground state by spin-orbital interaction.<sup>13</sup> In the present work we neglect this possibility.

Thus, the main anisotropic interactions in DIMPY are really simple to analyse. They include anisotropic  $g$ -tensor, which is the same for all magnetic ions of the given spin-ladder and a Dzyaloshinskii-Moria interaction, which is uniform along the leg of the ladder and the Dzyaloshinskii-Moria vectors are exactly opposite on the legs of the given ladder.

#### IV. EXPERIMENTAL RESULTS.

##### A. Angular dependence of the ESR absorption at 77 K.

We have taken rotational patterns of ESR absorption for the magnetic field applied in different crystallographic planes. Because of monoclinic lattice symmetry care should be taken with consistent determination of the field direction with respect to the lattice axes. We will use a cartesian basis with  $X||a$ ,  $Y||b$  and  $Z||c^*$  for the direction description. Rotation patterns were taken for the field confined to  $(XY)$  and  $(XZ)$  planes and to the plane containing  $Z$  axis and an  $(Y-X)$  direction. All rotation patterns were taken for more than 180° angular sweeps.

Examples of absorption spectra and angular dependences of the  $g$ -factor are shown of the Figure 2. We observe one or two Lorentzian absorption lines. These absorption lines are clearly due to the different spin ladders: the ladders are equivalent with respect to the magnetic field for  $\mathbf{H}||Y$  and  $\mathbf{H} \perp Y$ , and we observe single component absorption at these orientations. Anisotropy of  $g$ -factor is typical for the  $\text{Cu}^{2+}$  ion,  $g$ -factor varies

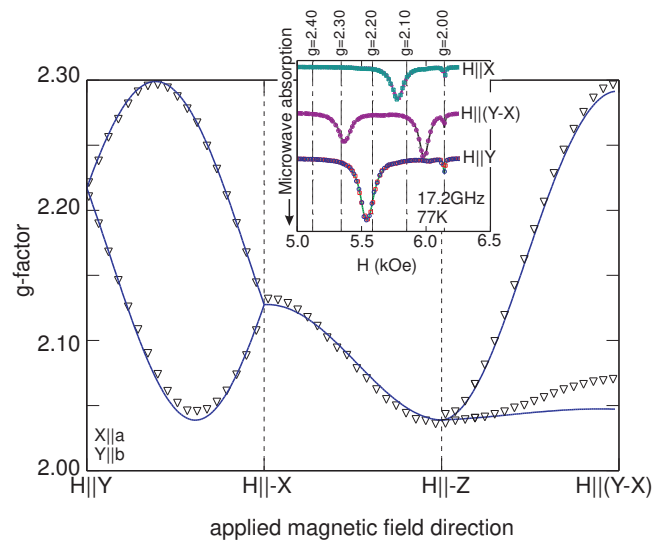


FIG. 2. (color online) Main panel: angular dependence of the  $g$ -factor at 77 K. Symbols - experimental data, curves - uniaxial  $g$ -tensor best fit (see text). Experimental error is about of 0.1% and is within symbol size. Inset: example of ESR absorption spectra at representative orientations. Symbols - experimental data, curves - best fit with Lorentzian lineshape, vertical lines corresponds to certain  $g$ -factor values. Narrow line with  $g = 2.00$  (at 6.13 kOe) is a DPPH marker.

from about 2.03 to 2.30 in agreements with powder ESR measurements of Ref.14

Angular dependence of the ESR linewidth was determined by fitting observed absorption spectra with a single Lorentzian line or with a sum of two Lorentzian lines (Fig.3). Typical half-width at half-height at 77 K was around 50 Oe. Field inhomogeneity in the used magnet and uncertainties of the fit procedure limit accuracy of the linewidth determination to about 5 Oe, however angular dependence is clearly present. We were able to cross-check our results at certain selected orientations on a commercial Bruker X-band spectrometer and we have found that X-band data are in agreement with our results.

##### B. Low-temperature ESR.

Low temperature (below 77 K) ESR absorption was measured at certain fixed field directions: for the field applied parallel to the symmetry axis  $\mathbf{H}||Y$  and for the field canted by approximately 45° towards  $X$  axis. In the first case both ladders are equivalently oriented with respect to the magnetic field, while the later case corresponds to the maximal difference of the ladders' effective  $g$ -factor, as evidenced by 77 K measurements.

As expected, we observe single-component ESR absorption for  $\mathbf{H}||Y$  and two resolved ESR signals from different ladders for the canted sample. Temperature evolution of the ESR absorption spectra is qualitatively

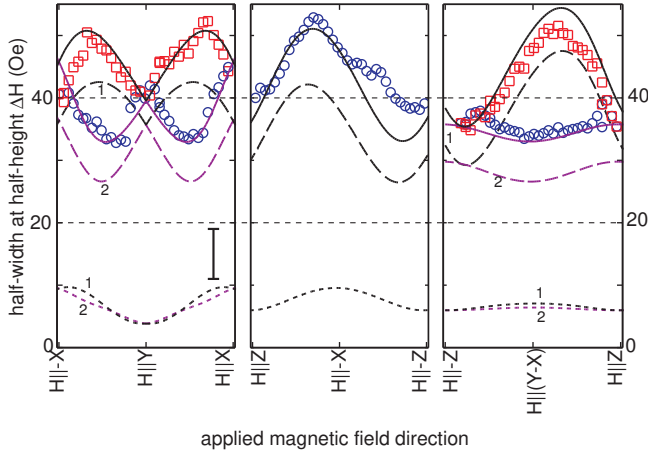


FIG. 3. (color online) Angular dependence of the ESR linewidth at  $f=17.2$  GHz,  $T=77$  K (half-width at half-height). Vertical bar at the left panel shows typical errorbar size (double error). Squares: width of the high- $g$  component. Circles: width of the low- $g$  component. Curves: model description (see text), solid lines show full linewidth, dashed and dotted lines show contributions due to DM and SAE interactions respectively. Marks "1" and "2" indicate contributions corresponding to the same ladder.

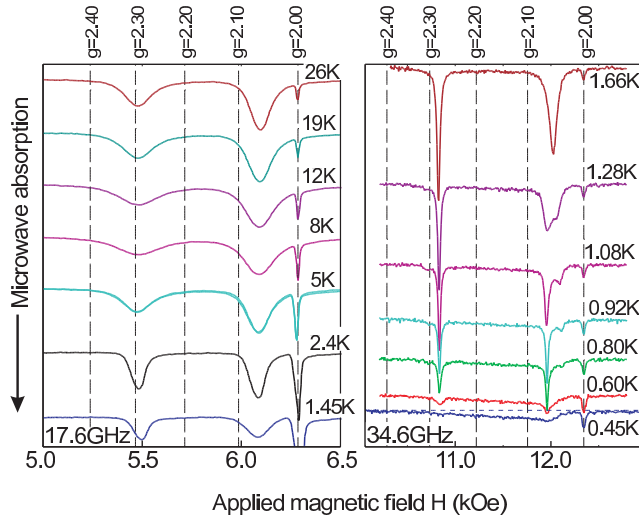


FIG. 4. (color online) ESR absorption spectra at low temperatures,  $\mathbf{H} \parallel (X+Y)$ . Vertical dashed lines mark resonance fields corresponding to the shown  $g$ -factor values. Horizontal dashed line at 0.45 K curve is a guide to the eye at zero-absorption level. Narrow absorption line at  $g=2.00$  is a DPPH marker.

similar in both cases (Figure 4). Below 10 K the ESR absorption intensity freeze down due to the presence of the energy gap. ESR signal continue to loose intensity down to 450 mK and almost vanishes at this temperature. Lowest temperature (450 mK) ESR absorption includes broad powder-like absorption spectrum probably related to the distorted surface of the sample.

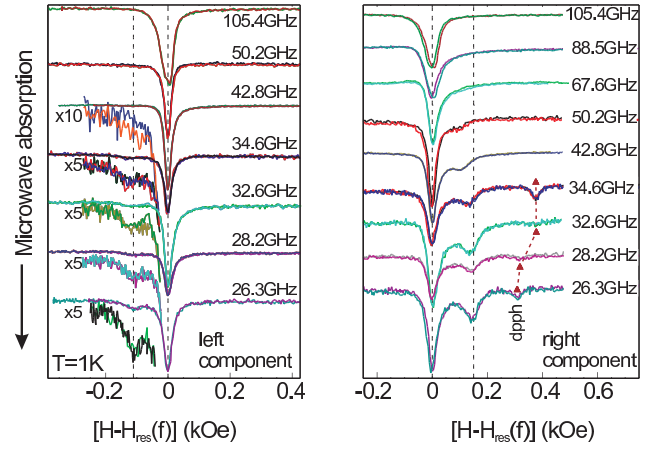


FIG. 5. (color online) ESR absorption spectra at the temperature  $T \approx 1$  K at different frequencies,  $\mathbf{H} \parallel (X+Y)$ . All spectra are shifted along the field axis to fit positions of the main absorption subcomponents. Left panel: left absorption component ( $g \approx 2.28$ ), weak absorption subcomponent is magnified by the factor of 5 or 10 for better presentation. Right panel: right absorption component ( $g \approx 2.05$ ). Vertical dashed lines mark positions of the absorption subcomponent at lowest frequency. Triangles on the right panel mark position of the DPPH marker absorption ( $g = 2.00$ ).

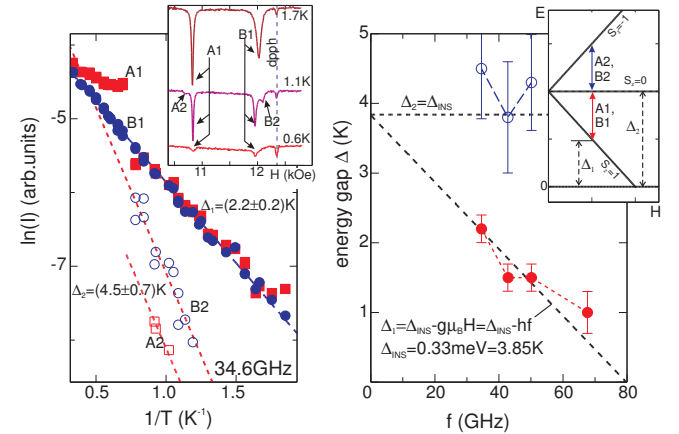


FIG. 6. (color online) Left panel: temperature dependence of the ESR intensity below 1 K at  $f=34.6$  GHz,  $\mathbf{H} \parallel (X+Y)$ . Inset: examples of ESR absorption and ESR components and subcomponents notations. Symbols - experimental data, dashed lines - fits with thermoactivation law  $I \propto \exp(-\Delta/T)$ . Right panel: dependence of the determined activation gaps for different spectral subcomponents. Filled symbols: intense A1 and B1 subcomponents, open symbols - weak A2 and B2 subcomponents. Lines: parameters-free model dependence calculated with the zero-field gap value  $\Delta_{INS}$  known from the inelastic neutron scattering experiments.<sup>9,10</sup> Inset: scheme of the energy levels of a spin-gap magnet in a magnetic field. Solid vertical arrows show transitions corresponding to the observed ESR absorption, dashed vertical arrows mark activation gaps for these transitions.



We did not observe any additional absorption signals which could be related to the formation of the field induced ordered phase above the critical field to appear at the lowest temperature of 450 mK in the fields up to 10 T at the frequencies of 26...35 GHz. This is in agreement with the known phase diagram of DIMPY<sup>11</sup> demonstrating that highest temperature of the transition into the ordered state is about 300 mK.

Additional splitting of the ESR absorption lines was observed around 1 K (Figure 5), resonance fields of the split sub-components differ by approximately 150 Oe. This splitting was observed at various frequencies, it was most pronounced on the high-field component of the canted sample ESR absorption spectra. One of the split sub-components is much weaker than the other and freeze out faster on cooling. Remarkably, mutual orientation of the weaker and stronger sub-components is different for the low-field and high-field components. We did not observe resolved splitting for the  $\mathbf{H}||Y$  orientation, instead a weak peak of the linewidth was observed around the same temperature of 1 K probably indicating unresolved splitting.

At low temperatures intensities of all components follow exponential law  $I \propto \exp(-\Delta/T)$  (Figure 6). Energy gap for the weaker sub-components is larger than that for the main sub-components. By taking temperature dependences of the ESR absorption at different frequencies we were able to determine the values of the energy gaps at several frequencies revealing dependence of the activation energy from the resonance field (Figure 6).

### C. ESR linewidth evolution from 300 K to 400 mK.

Temperature evolution of the ESR linewidth was measured from room temperature down to 400 mK (Figure 7). The temperature dependence is qualitatively similar in all orientations and demonstrate strongly non-monotonous behavior. At high temperatures (above 90 K) linewidth strongly increases with heating rising from about 50 Oe at 77 K to about 300 Oe at 300 K. On cooling below 77 K linewidth again increases reaching maximum at temperature  $T_{max} = 9.0 \pm 0.2$  K. Temperature of the maximum is the same for all orientations, while linewidth value at the maximum varies from 90 Oe to 140 Oe, both of the extreme values being observed in the orientation of maximal splitting  $\mathbf{H}||(X \pm Y)$  for different components of ESR absorption. Below  $T_{max}$  linewidth again decreases reaching its minimal value of about 10 Oe (observed at  $\mathbf{H}||Y$ ) at 2 K, which is most likely limited by the field inhomogeneity in our setup. On cooling below 2 K a peak in the linewidth is observed around 1 K. The peak is most pronounced for the high-field component in the orientation of maximal splitting of the ESR absorption components, peak position coincides with the temperature of subcomponents appearance. Similar but less pronounced peak is observed for  $\mathbf{H}||Y$ . High- $g$  component in the  $\mathbf{H}||(X + Y)$  orientation

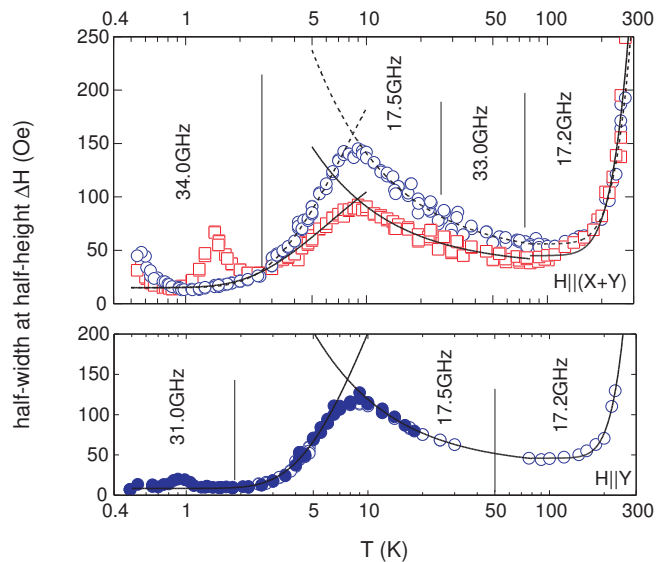


FIG. 7. (color online) Temperature dependence of the ESR linewidth. Upper panel:  $\mathbf{H}||(X + Y)$ . Circles: low-field (high- $g$ ) component, squares: high field (low- $g$ ) component. All data are measured on the samples from the same batch. Lower panel:  $\mathbf{H}||Y$ . Filled and open symbols corresponds to the data measured on samples from different batches. Experimental data were collected in different experimental setups operating at different frequencies, vertical lines mark approximate temperature boundaries for different experiments, microwave frequencies of each experiment are given. Typical errorbar size is around symbol size. Curves on both panels show empirical fit equations (see text and Table I).

does not demonstrate such a peak, which is probably related to the very low intensity of the appearing weaker subcomponent which cause fitting procedure to lock on the main spectral subcomponent. Finally, on cooling below 1 K linewidth of both components in the  $\mathbf{H}||(X + Y)$  orientation increases again.

## V. DISCUSSION.

### A. Recovery of the $g$ -tensor.

Observed angular dependences of the  $g$ -factor can be fitted assuming uniaxial  $g$ -tensor. As was described in the Section III  $g$ -tensor is the same for the given ladder and orientations of the  $g$ -tensors in inequivalent ladders are bound by 2-nd order axis. Hence, directions of the main axis can be expressed via polar angles as  $\mathbf{n}_{g1,2} = (\pm \sin \Theta \cos \phi; \cos \Theta; \pm \sin \Theta \sin \phi)$ , here we count polar angle  $\Theta$  from the 2-nd order axis  $Y||b$ , different signs corresponds to the different ladders.

Least squares fit of our data (see Figure 2) yields  $g$ -tensor components  $g_{||} = 2.296 \pm 0.010$  and  $g_{\perp} = 2.040 \pm 0.006$  and angles  $\Theta = (34.8 \pm 1.5)^{\circ}$  and  $\phi = (178 \pm 4)^{\circ}$ . Fit quality can be improved by assuming general form of the  $g$ -tensor. However, this results only in minor planar

anisotropy (with principal  $g$ -factor values of  $2.038 \pm 0.010$  and  $2.058 \pm 0.010$ ) which is on the edge of experimental error.

Main axis of the  $g$ -tensor within accuracy of our experiment lies in the  $(XY)$ -plane of the crystal. This seems to be accidental as there is no symmetry reasons to choose this plane in the monoclinic crystal. Orientation of the  $g$ -tensor main axes  $\mathbf{n}_{g1,2}$  with respect to the crystal structure is shown at the Figure 1. We can not decipher which of the orientations corresponds to different ladders.

Found values of the main  $g$ -tensor components coincide with the values found in earlier powder high-field ESR experiment.<sup>14</sup> The value of the  $g$ -factor for the  $\mathbf{H}||a$  case  $g_a = 2.17$  was found in Ref.11 by magnetization fit, this value disagree by 2% with the value  $g_a^{(ESR)} = 2.130 \pm 0.005$  found in our experiment.

### B. Interladder coupling estimation.

Anisotropy of the  $g$ -tensor opens a direct way to the estimation of interladder coupling. If the coupling between the ladders with different  $g$ -tensor orientation would be strong enough, then a common spin precession mode would be observed, a well known exchange narrowing phenomenon.<sup>15,16</sup>

Instead, we observe well resolved ESR absorption signals from the inequivalent ladders. Thus, upper limit on the interladder coupling can be estimated from the minimal splitting  $\Delta H$  observed, which is around 40 Oe at 17 GHz experiment (corresponds to components  $g$ -factor difference  $\Delta g = 0.015$  at Figure 2).

As it is known from the exchange narrowing theory, equally intense components with splitting  $\Delta\omega$  will form a common precession mode if the coupling strength is above  $J_c \simeq \hbar\Delta\omega$ . Hence we obtain an estimate  $J_{inter} < \hbar\nu \frac{\Delta H}{H_{res}} \simeq 5$  mK or about 0.5  $\mu$ eV.

This value is in reasonable agreement with the earlier estimate of the interladder exchange coupling from the ordered phase boundary calculated in mean-field approximation<sup>11</sup> as  $nJ'_{MF} = 6.3$   $\mu$ eV (here  $n$  is the number of coupled ladders, coupling considered to be equal in all directions). Note that our observation provides a direct estimate of the coupling between the unequivalently oriented ladders only.

### C. Linewidth temperature dependence.

Non-monotonous temperature dependence of the linewidth indicates that spin precession relaxation is governed by different processes in the different parts of the studied temperature range. We fit this temperature dependence by set of empirical equations as shown on Figure 7 and discussed below. Values of the fit coefficients for the empiric equations used are gathered in the Table I.

High temperature increase of the ESR linewidth (above 77 K) is naturally related to the spin-lattice relaxation: increase of the phonons population numbers leads to the increase of the relaxation rate. Linewidth dependences can be fitted by the sum of the constant contribution describing the high-temperature spin-spin relaxation and an empirical activation law  $\Delta H = \Delta H_0 + A \exp(-E_a/T)$ . Activation energy is  $E_a = (1400 \pm 150)K$ . Similar behavior with activation energy of the same order of magnitude was reported for other cuprates<sup>17,18</sup> and it was discussed<sup>18</sup> as a relaxation via excited state with a competing Jan-Teller distortion. However, detailed analysis of the lattice relaxation is beyond the scopes of the present paper.

Lattice contribution vanishes with cooling. Shallow minimum of the linewidth at 70-100 K indicates that phonon relaxation channel is practically frozen down here. Hence, we assume that linewidth measured at 77 K is mostly due to spin-spin relaxation.

It is well known<sup>19,20</sup> that anisotropic spin-spin interactions are responsible for the spin-spin relaxation. Thus, ESR linewidth provides access to determine these interactions strength. For the concentrated magnets Dzyaloshinskii-Moria interaction (which is allowed by the lattice symmetry of DIMPY) and symmetric anisotropic exchange interaction are the main contributions. Temperature dependence of the ESR linewidth is one of the physical effects to find which of these anisotropic interactions dominates the linewidth.

Detailed description of the ESR linewidth in a quantum spin-ladder is only emerging now: case of spin ladder with symmetric anisotropic spin-spin coupling was considered by recently by Furuya and Sato<sup>21</sup>, a theory accounting for the uniform Dzyaloshinskii-Moriya interaction is still to be constructed. Theory of an ESR linewidth for a quantum  $S = 1/2$  chain was developed by Oshikawa and Affleck more than decade ago.<sup>22</sup> We will apply their results to understand qualitatively temperature dependence of the ESR linewidth at high temperatures  $T \gg J_{leg, rung}$ . Oshikawa and Affleck have demonstrated that contribution of the symmetric anisotropic exchange interaction to the ESR linewidth (exchange anisotropy in their terms) decreases with cooling. They also considered contribution of the staggered Dzyaloshinskii-Moria interaction and have found that in this case ESR linewidth is increasing as  $1/T^2$  at low temperatures. Oshikawa and Affleck demonstrated that at high temperature limit staggered Dzyaloshinskii-Moria interaction results in the linewidth increasing with cooling as  $1/T$ . As the high-temperature linewidth is determined by the pair spin correlations, this result should be actually the same for the staggered and uniform Dzyaloshinskii-Moria interaction. This conclusion is in agreement with the results of Ref.17 for the uniform Dzyaloshinskii-Moria interaction in quasi one dimensional antiferromagnet  $\text{Cs}_2\text{CuCl}_4$ . Thus, increase of the linewidth with cooling below 80 K is a direct indication of the dominating role of the Dzyaloshinskii-Moria

TABLE I. ESR linewidth empirical fit equations parameters in different temperature ranges and at different orientations. For the orientations with two ESR components resolved (LF) and (HF) marks fit results for the low-field and high-field components correspondingly, (HF+LF) marks cases where linewidths of both components are close and their temperature dependences are fitted jointly.

Temperature range and fit eqns.	Parameters	Typical fit accuracy	$\mathbf{H}  Y$	$\mathbf{H}  (x+y)$	$\mathbf{H}  (y+z)$
$T > 80$ K	$\Delta H_0$ , Oe	$\pm 5$ Oe	46	45 (HF); 56 (LF)	
$\Delta H = \Delta H_0 + A \exp(-E_a/T)$	$A, \times 10^4$ Oe	$\pm 50\%$	5.9	1.7 (HF); 1.8 (LF)	
	$E_a$ , K	$\pm 150$ K	1510	1240 (HF); 1310 (LF)	
$15\text{K} < T < 80$ K	$\Delta H_\infty$ , Oe	$\pm 5$ Oe	35	35 (HF); 44(LF)	40 (HF+LF)
$\Delta H = \Delta H_\infty(1 + \Theta/T)$	$\Theta$ , K	$\pm 3$ K	24	16 (HF); 22(LF)	14 (HF+LF)
$1.5\text{K} < T < 7$ K	$\Delta H_0$ , Oe	$\pm 2$ Oe	10	15 (HF); 15 (LF)	15(HF+LF)
$\Delta H = \Delta H_0 + A \exp(-E_a/T)$	$A, \times 10^2$ Oe	$\pm 30\%$	6.4	1.7 (HF); 3.9 (LF)	5.3 (HF+LF)
	$E_a$ , K	$\pm 1.5$	14 (9.6 <sup>a</sup> )	6.4 (HF); 8.4 (LF)	10.5(HF+LF)

<sup>a</sup> Value of  $E_a = 9.6$  K corresponds to the best fit with fixed parameter  $\Delta H_0 = 0$  (see text).

interaction for the spin relaxation processes in DIMPY. To model first order of the  $1/T$  expansion we fit our data by the law  $\Delta H = \Delta H_\infty(1 + \Theta/T)$ . Characteristic temperature  $\Theta$  is anisotropic and varies from 15 to 25 K in the orientations presented on the Figure 7. This temperature scale is close to the exchange integral value in agreement with the results of Refs.22,17.

The crude estimate of this interaction strength can be obtained from the linewidth at 80 K, which is approximately 50 Oe. As this temperature far exceeds the exchange integral scale high-temperature approximation can be used. We will discuss exact calculations below while describing angular dependence, but as an estimate one can write  $\hbar\Delta\omega \sim \frac{D^2}{J}$  or  $D \sim \sqrt{g\mu_B\Delta H J} \sim 0.3$  K.

As the temperature decreases below approximately 10 K linewidth start to decrease. This decrease is naturally related to the gapped spectrum of the spin ladder. At low temperatures magnetic properties of a spin ladder can be described on the triplet quasiparticles language and linewidth is then interpreted as an inverse lifetime of these quasiparticles, which is partially determined by their interaction. As temperature approaches scale of the energy gap, quasiparticles population numbers decreases, gas of the quasiparticles became diluted and quasiparticles interaction contribution froze out. This results in the narrowing of the ESR absorption line with cooling. The linewidth temperature dependence indeed follows thermoactivation law  $\Delta H = \Delta H_0 + A \exp(-E'_a/T)$  with activation energy  $E'_a = 6.4...14$  K in different orientations.

If the relaxation processes would be due to the pair interaction of quasiparticles, the relaxation rate would be proportional to the quasiparticles concentration squared and the activation energy would be about  $2\Delta_0$ , where  $\Delta_0 = 0.33$  meV (or 3.8 K) is a zero-field gap. The activation energies for  $\mathbf{H}||(X+Y)$  orientation are close to this expectation. However, for the field applied along the second-order axis  $\mathbf{H}||Y$  the best fit activation energy ( $14 \pm 1.5$  K) far exceeds the doubled zero-field gap value.

Most likely this result is an artefact due to the effects of field inhomogeneity in our experimental setup: the low temperature linewidth is minimal for  $\mathbf{H}||Y$  and could be limited by experimental resolution. This leads to overestimation of  $\Delta H_0$  parameter which in turn results in overestimation of the activation energy. Tentative fit of the  $\mathbf{H}||Y$  data with  $\Delta H_0$  value fixed to zero yields activation energy of 9.6 K which is much closer to twice zero-field gap value. Similar  $\Delta H_0 = 0$  fits in other orientations lead to the smaller corrections of the determined activation energy.

Thus, within accuracy of our experiment, which is mostly limited by field inhomogeneity of the magnetic field in the superconducting coil used, we can conclude that pair quasiparticles interactions dominates spin-spin relaxation processes of the spin-ladder in low-temperature regime.

The peak of the linewidth around 1 K is related to the splitting of the ESR lines into subcomponent, its origin is related to the classical exchange narrowing phenomenon.<sup>15,16</sup> The exchange frequency became temperature dependent being related to the quasiparticles concentration. At low temperatures (low quasiparticles concentration) split ESR line is observed, at higher temperatures (higher quasiparticles concentration) effective exchange interaction between the quasiparticles gain efficiency and a common precession mode is formed. Crossover between these regimes results in the broadening of ESR line. Similar effect is observed in other spin-gap magnets<sup>23,24</sup> and in other systems.<sup>25</sup>

Finally, definitive increase of the linewidth below 700 mK is probably indicative of the critical regime in the vicinity of the field induced phase transition.

#### D. Angular dependence of the ESR linewidth.

According to the theory of the exchange narrowed resonance spectra<sup>26,27</sup>, the half width at half maximum for a single Lorentzian shaped line is given by

$$\Delta H = C \left[ \frac{M_2^3}{M_4} \right]^{1/2}, \quad (2)$$

where  $C$  is dimensionless constant of order unity, depending on how the wings of Lorentzian profile drop at fields of the order of exchange field ( $J/g\mu_B \ll \Delta H$ )<sup>27</sup>;  $M_2$  and  $M_4$  are the second and fourth moments of resonance line, firstly introduced by Van Vleck<sup>28</sup>

$$M_2 = \frac{\langle [\mathcal{H}_{anis}, S^+][S^-, \mathcal{H}_{anis}] \rangle}{h^2 \langle S^+ S^- \rangle}, \quad (3)$$

$$M_4 = \frac{\langle [\mathcal{H}_{ex}, [\mathcal{H}_{anis}, S^+]] [[S^-, \mathcal{H}_{anis}], \mathcal{H}_{ex}] \rangle}{h^4 \langle S^+ S^- \rangle}. \quad (4)$$

where  $S^\pm$  denote left/right circular components of the total spin summed up over the whole sample,  $\mathcal{H}_{ex}$  is isotropic exchange Hamiltonian,  $\mathcal{H}_{anis}$  is anisotropic one that doesn't commute with  $\mathcal{H}_{ex}$  hence causing broadening of the resonance line.

Analysis of the ESR linewidth based on calculation of the spectral moments is a well developed method which allows to identify nature of spin-spin interactions and estimate their magnitudes in magnetically concentrated systems.<sup>29</sup> Its benefit is that in high temperature limit ( $T \rightarrow \infty$ ) an exact expression for linewidth can be found out for an arbitrary spin system, whatever space dimension and exchange couplings.<sup>20,30</sup>

In the present paper we apply the "method of moments" to a strong-leg spin ladder system, described by Hamiltonian (1) with uniform Dzyaloshinskii-Moriya interaction

$$\mathcal{H}_{DM} = \sum_i \sum_{l=1,2} \mathbf{D}_l [\mathbf{S}_{l,i} \times \mathbf{S}_{l,i+1}], \quad (5)$$

here  $i$  enumerates rungs of the ladder and  $l$  enumerates legs of the ladder, DM vectors on the legs are considered arbitrary for the moment ( $\mathbf{D}_1 \neq \mathbf{D}_2$ ). Substituting Eq. (5) into Eqs.(3), (4) and using the corresponding commutation relations for  $S = 1/2$  spin operators, for the linewidth Eq. (2) in high temperature limit we have

$$\Delta H_\infty^{DM}(Oe) = C \sum_{l=1,2} \frac{[D_x^2 + D_y^2 + 2D_z^2]_l}{4\sqrt{2}\mu_B \tilde{J}_D g(\theta, \phi)} \quad (6)$$

where  $\tilde{J}_D = \sqrt{J_{leg}^2 + 2J_{rung}^2}$  mean an average exchange integral,<sup>30</sup> and angular dependence is determined by the transformation for DM vector

$$\begin{aligned} D_x &= D_X \cos \beta \cos \alpha + D_Y \cos \beta \sin \alpha - D_Z \sin \beta, \\ D_y &= D_Y \cos \alpha - D_X \sin \alpha, \\ D_z &= D_X \sin \beta \cos \alpha + D_Y \sin \beta \sin \alpha + D_Z \cos \beta. \end{aligned} \quad (7)$$

Here angles  $\alpha$  and  $\beta$  define orientation of the local coordinate system  $(x, y, z)$  where Zeeman term in Eq. (1) takes diagonal form  $g\mu_B H S^z$  with

$$g = \sqrt{A^2 + B^2 + C^2}, \quad (8)$$

where

$$\begin{aligned} A &= g_{XX} \sin \Theta \cos \phi + g_{XY} \cos \Theta + g_{XZ} \sin \Theta \sin \phi, \\ B &= g_{YX} \sin \Theta \cos \phi + g_{YY} \cos \Theta + g_{YZ} \sin \Theta \sin \phi, \\ C &= g_{ZX} \sin \Theta \cos \phi + g_{ZY} \cos \Theta + g_{ZZ} \sin \Theta \sin \phi \end{aligned}$$

and

$$\cos \alpha = \frac{A}{\sqrt{A^2 + B^2}}, \cos \beta = \frac{C}{\sqrt{A^2 + B^2 + C^2}},$$

here polar  $\Theta$  and azimuthal  $\phi$  angles define the direction of external magnetic field, so that  $\Theta$  and  $\phi$  are counted from  $Y$  and  $X$  axes, respectively, as during the  $g$ -tensor recovery procedure.

Note that by setting  $J_{rung} = 0$  and  $\mathbf{D}_1 = \mathbf{D}_2$  in Eqn. (6) we immediately arrive to the known result for 1D Heisenberg chain with uniform DM interaction [see formula (16) in Ref. 17].

DIMPY has two inequivalent ladders with different  $g$ -tensors and DM vectors. In accordance with crystal symmetry of the DIMPY (see Sec. III), the legs within same ladder are linked by inversion, so that

$$\hat{\mathbf{g}}_1^{(k)} = \hat{\mathbf{g}}_2^{(k)}, \mathbf{D}_1^{(k)} = -\mathbf{D}_2^{(k)}, (k = 1 \text{ or } 2), \quad (9)$$

here upper index ( $k = 1, 2$ ) denotes the inequivalent ladders and lower index enumerate legs of the ladder. The legs of inequivalent ladders are linked by screw rotation along the second order axis, hence

$$\begin{aligned} \mathbf{D}_l^{(2)} &= C_2(Y) \mathbf{D}_l^{(1)}, \\ \hat{\mathbf{g}}_l^{(2)} &= C_2(Y) \hat{\mathbf{g}}_l^{(1)} C_2(Y)^{-1}, (l = 1, 2), \end{aligned} \quad (10)$$

Orientation of the local axes is essentially different for inequivalent spin ladders. Having known directions of the main axes of  $g$ -tensors (see Sec. V A), it's easy to find their components referred to crystallographic axes

$$\hat{g}^{(1,2)} = \begin{pmatrix} 2.128 & \mp 0.12 & -0.008 \\ \mp 0.12 & 2.214 & \pm 0.005 \\ -0.008 & \pm 0.005 & 2.038 \end{pmatrix}, \quad (11)$$

where upper(down) sign corresponds to the ladder with upper(down) sign of  $\mathbf{n}_g$ .

Simulation of experimental data on the linewidth angular dependence by Eq. (6) showed that the Dzyaloshinskii-Moria interaction describes the angular variation of the linewidth in DIMPY well enough (within experimental error). However model including Dzyaloshinskii-Moria interaction only predicts value of linewidth which is systematically less than the experimental values by about 12 Oe. This fact indicates



there is an additional (small compared to DM interaction) source of the line broadening in DIMPY. The modelled values of the linewidth can be reconciled with the experimental ones by adding isotopic contribution  $\Delta H_0 = 12$  Oe, which can be probably ascribed to the residual spin-lattice relaxation, or by considering other anisotropic spin-spin couplings. Contribution to the linewidth from dipole-dipole interaction is quite small for DIMPY and at the shortest distance between Cu ions ( $r = a \approx 7.5$  Å) following conventional estimation<sup>31</sup> it does not exceed  $\sim 0.5$  Oe. Additional broadening in DIMPY can be related to SAE interaction along legs and rungs of the spin ladders which usually appear as further sources of ESR line broadening beyond the dominant DM interaction.<sup>17,32</sup> The contribution to the linewidth due to SAE interaction is derived in Appendix A.

Taking into account symmetry relations (Eqs. (9), (10), (11), (A3)) and, for definiteness setting  $\mathbf{D}_1^{(1)} = \mathbf{D}$ ,  $\hat{\mathbf{A}}_1^{(1)} = \hat{\mathbf{A}}$ , the fitting of linewidth angular dependence yields  $D_X = 0.15$ ,  $D_Y = -0.14$ ,  $D_Z = 0.075$  K and almost diagonal exchange-tensor with components  $J_{XX} = 0.08$ ,  $J_{YY} = -0.03$ ,  $J_{ZZ} = -0.05$ ,  $J_{XY} = -0.015$  K and  $J_{XZ} = J_{YZ} = 0$ . During simulation the Lorentzian profile with exponential wings was assumed, which implies  $C = \pi\sqrt{2}$ .

Directions of the found  $\mathbf{D}$  vectors are shown on the Figure 1. Components of the DM vector and SAE tensor given above correspond to the ladder with the  $g$ -tensor main axis orientation  $\mathbf{n}_{g1} = (\sin \Theta \cos \phi; \cos \Theta; \sin \Theta \sin \phi) \approx (-0.57; 0.82; 0)$  (when comparing with Fig.1 note that  $\mathbf{n}_g$  and  $-\mathbf{n}_g$  are physically equivalent), angle between  $\mathbf{D}$  and  $\mathbf{n}_g$  vectors (reduced to  $(-\frac{\pi}{2}; \frac{\pi}{2})$  range for convenience) is approximately  $23^\circ$ . Magnitude of the obtained Dzyaloshinskii-Moria vector  $|\mathbf{D}| = 0.22$  K agrees well with the crude estimation above (section VC).

As it is seen from Fig. 3, taking into consideration only an exchange mechanisms of spin anisotropy within the legs of ladders gives a good compliance with experiment. However, it is necessary to stress out, that without DM interaction SAE coupling only (see Appendix A) totally failed to give a correct description of the angular dependence of linewidth in DIMPY.

Our simulation shows that absolute value as well as angular anisotropy of the linewidth are predominantly attributed by DM interaction, while contribution to the linewidth due to SAE interaction is relatively small compared to DM one and gives a weak angular variation. Similar behavior of ESR linewidth with coexistent contributions from DM and SAE interactions within  $S = 1/2$  antiferromagnetic chains was observed in high symmetry crystal structure  $\text{KCuF}_3$ <sup>32</sup>.

The found DM vector have not only transverse but also nonzero *longitudinal* (with respect to the Cu-Cu exchange bond) component within the legs. Such result doesn't contradict with the general rules for DM vector, established by Moriya<sup>33</sup> based on general symmetry grounds for a pair of exchange interacting ions. More-

over, a simple analysis of the recovered  $g$ -tensors (see Sec. VA) leads to the same conclusion about direction of the DM vector. Since the axial component of the  $g$ -tensor has a maximal value, then the ground state orbitals of  $\text{Cu}^{2+}$  ions (typically " $\tilde{x}^2 - \tilde{y}^2$ "-like symmetry and  $\tilde{z}||\mathbf{n}_g$ ) should predominantly lie within the plane perpendicular to the main axis of a  $g$ -tensor, because the maximal matrix element ( $\langle \tilde{x}^2 - \tilde{y}^2 | l_g | \tilde{x}\tilde{y} \rangle = -2i$ ) relevant to spin-orbital coupling appears only in the case when an external magnetic field is applied parallel to the main axis of  $g$ -tensor. For the same reason an effective DM vector predominantly should lie along the main axis of the  $g$ -tensor. It should be noted that conventional rule determining DM vector as  $\mathbf{D} \propto [\mathbf{n}_1 \times \mathbf{n}_2]$ ,<sup>34,35</sup> where  $\mathbf{n}_1$  and  $\mathbf{n}_2$  are unit vectors connecting a exchange interacting ions with bridging ion, is not applicable in present case. Possible failure of this rule was mentioned before in Ref. 36, referring to the features of exchange process through a two bridging ions, which is also the case of DIMPY (see Fig. 1).

Thus, analysis of ESR linewidth allowed us to conclude that the DIMPY is a rare case of compound in which DM vector has a component along the line connecting the pair of exchange interacting ions. This is a consequence of low crystal symmetry of DIMPY and nontrivial orbital ordering.

#### E. Low-temperature sub-components appearance.

First, we recall main observations on the subcomponent appearance. ESR components splits around 1 K into two sub-components, one of which is much weaker. The splitting is best observed at  $\mathbf{H}||(\mathbf{X} + \mathbf{Y})$  orientation. Position of the weaker sub-component with respect to the stronger sub-component is different for both ESR absorption components. Maximal splitting is about 150 Oe and it decreases as the resonance field approaches critical field, weaker subcomponent became unresolvable at the fields above 2/3 of the critical field. Activation energies for the stronger and weaker subcomponents are different.

All these observations can be explained as an effect of the zero field splitting of triplet sublevels. This effect was already observed for various spin-gap magnets, e.g.  $\text{TiCuCl}_3$ ,<sup>23</sup> or  $\text{PHCC}$ .<sup>24</sup> Anisotropic interactions lift degeneracy of the  $S = 1$  triplet state and frequencies of the dipolar transitions  $|S^z = +1\rangle \leftrightarrow |S^z = 0\rangle$  and  $|S^z = -1\rangle \leftrightarrow |S^z = 0\rangle$  would become different. Here we assume, which is perfectly valid for the case of DIMPY, that the anisotropy is very small and spin projection on the field direction  $S^z$  can be considered as a good quantum number. Therefore, in the presence of such an anisotropy the resonance fields for  $|S^z = +1\rangle \leftrightarrow |S^z = 0\rangle$  and  $|S^z = -1\rangle \leftrightarrow |S^z = 0\rangle$  transitions in the constant frequency ESR experiment would differ and ESR absorption split into two sub-components.

Observed difference of the activation energies for the absorption sub-components and dependence of the acti-

vation energy on the microwave frequency used in the experiment is a direct consequence of this explanation. The ESR intensity at low temperature is determined by the population of the lowest sublevel. Hence, for the  $|S^z = +1\rangle \leftrightarrow |S^z = 0\rangle$  transition the activation energy is  $\Delta \approx \Delta_0 - g\mu_B H_{res} = \Delta_0 - h\nu$ , being determined by the population of the  $|S^z = +1\rangle$  sublevel (energy of this sublevel decrease with field, see inset on Figure 6). In the same time the activation energy for the  $|S^z = -1\rangle \leftrightarrow |S^z = 0\rangle$  remains constant (and equal to  $\Delta_0$ ) since the energy of  $|S^z = 0\rangle$  sublevel is field independent. The dependences of the activation energy on the microwave frequency of the ESR experiment are described by this model parameter-free using the zero-field gap value of 0.33 meV from the inelastic neutron scattering experiment.<sup>9,10</sup>

Behaviour of the sublevels of the spin-gap magnet in the vicinity of the critical field is a long-discussed problem. There is a general macroscopic (or bosonic) approach of Refs. 3, 5 and a 1D fermionic approach of Tsvelik<sup>4</sup> developed for the spin-chains. Fermionic model of Tsvelik yields results formally equivalent to the results of perturbation treatment of anisotropic interactions.<sup>37</sup> Thus, within these approaches the sublevels behave linearly in the vicinity of the critical field and the splitting of the ESR subcomponent should be then field independent. Bosonic model, on the contrary, predicts square-root-like approach to the critical field for the low-energy sublevel, while field dependence of the high-energy sublevel remains linear in the vicinity of the critical field. Therefore, sub-components splitting will change close to the critical field. However, this nonlinearity of the bosonic model extends only in the small vicinity of the critical field ( $H_c - H$ )  $\sim \Delta E/\mu_B \sim \Delta H$ , here  $\Delta E$  is the zero field triplet sublevels splitting and  $\Delta H \simeq 150$  Oe is the observed sub-components splitting. We observe (Figure 5) that the observed splitting is halved (compare 50.18 GHz and 26.30 GHz curves at the Figure 5) in the field of about 2/3 of the critical field ( $H_c \simeq 30$  kOe, zero-field gap of 0.33 meV corresponds to the frequency of 80 GHz), i.e. well below this nonlinearity range. This probably indicates that field evolution of the split sub-components follows some other laws on approaching the critical field. Similar behaviour of the ESR line split by the uniform Dzyaloshinskii-Moria interaction was recently reported for a quasi-1D antiferromagnet  $\text{Cs}_2\text{CuCl}_4$ .<sup>38</sup>

Under an assumption that the uniform Dzyaloshinskii-Moria interaction along the legs of the ladder is responsible for the observed splitting, anisotropy axis have to be aligned along the  $\mathbf{D}$  vector. We calculated effects of the DM coupling perturbatively for the limiting case of strong-rung ladder (see Appendix B). Interdimer DM interaction mixes one and two-particle excited  $S^z = \pm 1$  states which results in the triplet sublevels splitting by  $\delta E = \frac{D^2}{2J}$ ,  $S^z = \pm 1$  sublevels being shifted down. This corresponds to the easy-axis anisotropy for the triplet excitations,  $\mathbf{D}$  direction being the easy axis direction. Taking the magnitude of the DM vector  $D \approx 0.20$  K

as estimated from the high-temperature ESR linewidth analysis and substituting energy gap of 0.33 meV as an exchange parameter of the perturbative model we obtain an estimate of the sublevels splitting  $\delta E \simeq 5$  mK which corresponds to sub-components splitting of about 40 Oe, factor of four less then the experimentally observed value. However, perturbative treatment starting from the uninteracting dimers is at best a qualitative model for a strong-leg ladder and a detailed description of a strong-leg spin ladder with uniform Dzyaloshinskii-Moria interaction needs a separate theoretical effort.

We can not unambiguously determine type of the anisotropy from our experimental observation since our setup does not allow to take an angular dependence at He-3 temperature range. However, as it is known from the formally similar problem of  $S = 1$  ion in a crystal field<sup>19,20</sup> the effective anisotropy constant changes monotonously with field rotating away from the anisotropy axis  $C_{eff} = \frac{C}{2} (3 \cos^2 \xi - 1)$ , where  $\xi$  is an angle counted from the anisotropy axis  $z$  and anisotropy  $C$  enters spin Hamiltonian as  $C(S^z)^2$ . It is maximal at the field parallel to the anisotropy axis, it change sign and decreases by the factor of two at the orthogonal orientation of the magnetic field and it turns to zero at a magic angle. Thus, as splitting observed for the high-field component is larger then that from the low-field component (approximately 150 Oe vs. 110 Oe, see Figure 5) and weaker sub-component is located on different side from the main sub-component, we find it more likely that the high-field component corresponds to the ladder with the magnetic field close to the true anisotropy axis. In this case, as for the field applied close to anisotropy axis the weaker subcomponent is located to the right from the stronger subcomponent, the splitting of the triplet sublevels follows easy-axis type of anisotropy energy of  $S^z = \pm 1$  states being lower then energy of  $S^z = 0$  state in zero field.

However, this tentative identification of the anisotropy axis deviates from the simple model of DM interaction only: as the vectors  $\mathbf{D}$  and  $\mathbf{n}_g$  are quite close for the given ladder the low-field component (corresponding to the higher longitudinal  $g$ -factor) should then be closer to the anisotropy axis. Possible reason for this deviation is the effect of symmetric anisotropic exchange on the rungs of the ladder (see Appendix B). SAE coupling is smaller in magnitude, but it enters to the triplet sublevels splitting linearly, why DM contribution is quadratic. This is contrary to the linewidth calculations where both couplings enter quadratically. Thus, description of the sub-components splitting probably lies beyond the simple model with DM interaction only and requires accounting for other anisotropic interactions.

## VI. CONCLUSIONS.

The strong-leg spin ladder system DIMPY is an established test example of the Heisenberg spin ladder. How-

ever, anisotropic spin-spin interactions, and in particular Dzyaloshinskii-Moria interaction of intriguing geometry: uniform along the leg of the ladder and exactly opposite on the other leg, give rise to a family of interesting phenomena.

We have estimated parameters of Dzyaloshinskii-Moria interaction from high-temperature data. We observe splitting of the ESR line at low temperatures which is related to the zero-field splitting of the triplet sublevels by the same interaction. Finally, we observe series of crossovers between different regimes of relaxation of spin precession on cooling from room temperature to 400 mK.

We present qualitative explanations of our observations. Simple geometry of the exchange couplings and anisotropic spin-spin interactions makes DIMPY one of the few candidates for the model-free microscopic description of the effects of anisotropic interactions on the properties of a spin-gap magnet, which is still awaiting for a theoretical effort.

### ACKNOWLEDGMENTS

We thank A.B.Drovosekov (Kapitza Institute) for the assistance with ESR experiment above 77 K and Prof.A.K.Vorobiev (M.Lomonosov Moscow State University) for the possibility to perform reference measurements with X-band spectrometer. We thank K.Povarov, Prof. M.V.Eremin and Prof. A.I.Smirnov for valuable and stimulating discussions. Authors acknowledge usage of "Balls & Sticks" software to build crystal structure images.

The work was supported by Russian Foundation for Basic Research Grant No.15-02-05918, Russian Presi-

dential Grant for the Support of the Leading Scientific Schools No.5517.2014.2. M .F. work was supported by the Russian Government Program of Competitive Growth of Kazan Federal University. This work was partially supported by the Swiss National Science Foundation, Division 2.

### Appendix A: Linewidth contribution by a SAE interaction along the legs.

Symmetric anisotropic exchange (SAE) coupling is allowed both on the rungs and on the legs of the ladder. Our aim here is to demonstrate that SAE coupling can explain contribution of about 20% of the total linewidth that can not be described by DM coupling alone. We will focus here on a SAE coupling along the legs of the ladder. We have checked that a SAE coupling along the rung yields similar angular dependence and its contribution differs only by some numerical scaling factor. However we expect that contribution of the SAE couplings on the rungs should be small in a strong-leg ladder since the overlapping of the orbitals along the rung is smaller.

An expression for ESR linewidth due to a SAE coupling along the legs of spin ladder is derived similarly as was done for a DM one in Sec. V D, applying

$$\mathcal{H}_{SAE} = \sum_i \sum_{l=1,2} \mathbf{S}_{l,i} \hat{\mathbf{A}}_l \mathbf{S}_{l,i+1} \quad (\text{A1})$$

to the Eqs.(3), (4), (2) in the framework of "method of moments", that in the high temperature limit of  $S = 1/2$  leads to

$$\Delta H_\infty^{SAE} = C \sum_{l=1,2} \frac{[(2\lambda_{zz} - \lambda_{xx} - \lambda_{yy})^2 + 10(\lambda_{xz}^2 + \lambda_{yz}^2) + (\lambda_{xx} - \lambda_{yy})^2 + 4\lambda_{xy}^2]_l}{8\sqrt{6}\mu_B \tilde{J}_S g(\theta, \phi)}, \quad (\text{A2})$$

where  $\tilde{J}_S = \sqrt{J_{leg}^2 + 2/3 J_{rung}^2}$ , and the exchange-tensor components in the local coordinates,  $\lambda_{\eta\gamma}(\alpha, \beta)$ , ( $\eta, \gamma = x, y, z$ ) are defined by transformation given in Ref. 13 [see formulae A2-A4 therein] and, as usually, are expressed via the intrinsic exchange parameters  $J_{\mu\tau}$  of symmetric tensor  $\hat{\mathbf{A}}$  in crystallographic coordinates ( $\mu, \tau = X, Y, Z$ ).

In accordance with crystal symmetry of the DIMPY (see Sec. III), symmetrical exchange tensors on the legs of same ladder are equal, while on the legs of inequivalent ladders they are related by a screw rotation along the second order axis, that is

$$\begin{aligned} \hat{\mathbf{A}}_1^{(k)} &= \hat{\mathbf{A}}_2^{(k)}, \quad (k = 1 \text{ or } 2) \\ \hat{\mathbf{A}}_l^{(2)} &= C_2(Y) \hat{\mathbf{A}}_l^{(1)} C_2(Y)^{-1}, \quad (l = 1, 2) \end{aligned} \quad (\text{A3})$$

Generally, taking into account relation of  $J_{\eta\gamma} = J_{\eta\gamma}$  for

a symmetric tensor, an exchange tensor has six different components, constrained by  $Tr J_{\eta\gamma} = 0$  condition. However, since the anisotropy of the  $g$ -tensor and the tensor of SAE coupling originates from the same spin-orbital interactions, accidental smallness of  $g_{XZ}$  and  $g_{YZ}$  components allows to assume  $J_{XZ} = J_{YZ} = 0$  during the fitting procedure. We have found, that the remaining four components of the SAE tensor are enough to reproduce our data.

## Appendix B: Perturbative treatment of triplet sublevels splitting by uniform DM and SAE couplings.

Strong-rung  $J_{rung} \gg J_{leg}$  limit allows to use wavefunctions of the isolated dimers as a zero-order approximation. For the dimer located at the  $n$ -th rung wavefunction of the ground state is  $\psi_{n0} = \frac{1}{\sqrt{2}}(|\uparrow\downarrow\rangle_n - |\downarrow\uparrow\rangle_n)$  and wavefunctions of the excited triplet are  $\psi_{n11} = |\uparrow\uparrow\rangle_n$ ,  $\psi_{n10} = \frac{1}{\sqrt{2}}(|\uparrow\downarrow\rangle_n + |\downarrow\uparrow\rangle_n)$  and  $\psi_{n1-1} = |\downarrow\downarrow\rangle_n$ . Wavefunction of the collective ground state is  $\Psi^{(0)} = \prod_p \psi_0^{(p)}$  and single-particle excited states with the excitation at the  $n$ -th dimer can be build as

$$\Psi_{n11}^{(1)} = \prod_{p=0}^{n-1} \psi_{p0} \times \psi_{n11} \times \prod_{p=n+1}^N \psi_{p0} \quad (B1)$$

and similarly for other spin projections. Many-particle excited state can be constructed similarly keeping in mind hard-core repulsion as only one excited state per dimer is allowed.

One-particle states are  $N$ -fold degenerated, this degeneration will be lifted by interdimer exchange coupling  $J_{leg}$  giving rise to excitations dispersion.

We consider effect of interdimer DM interaction (5) with DM vectors oppositely aligned on the legs of the ladder. This configuration conserves symmetry axis (direction of the DM vector, which we will use as  $z$ -direction), thus excitations will have well defined  $S^z$  values. Interdimer DM interaction can then be expressed as

$$V = \frac{D}{2l} \sum_n [S_{1,n}^- \hat{S}_{1,n+1}^+ - S_{1,n}^+ S_{1,n+1}^- - S_{2,n}^- \hat{S}_{2,n+1}^+ + S_{2,n}^+ S_{2,n+1}^-] \quad (B2)$$

By applying this operator to the ground state and to one-particle excited states we obtain

$$V\Psi^{(0)} = 0 \quad (B3)$$

$$V\Psi_{n10}^{(1)} = 0 \quad (B4)$$

$$V\Psi_{n11}^{(1)} = \frac{D}{2l} (-\Psi_{n10;(n+1)11}^{(2)} + \Psi_{n10;(n-1)11}^{(2)}) \quad (B5)$$

here  $\Psi_{n10;m11}^{(2)}$  are two-particle excited states with  $S = 1, S^z = 0$  excitation on the  $n$ -th rung and  $S = 1, S^z = 1$  excitation on the  $m$ -th rung.

Thus, interdimer DM interaction mixes  $S^z = \pm 1$  single particle excited states with  $S^z = \pm 1$  two particle excited states. This mixing results in the second-order perturbative correction to the energy of the single-particle state

$\delta E = -\frac{D^2}{2J_{rung}}$ ,  $S^z = \pm 1$  being shifted down. As this correction is the same for all  $S^z = \pm 1$  states, weak interdimer Heisenberg coupling  $J_{leg}$  will not affect it.

This result differs from the effect of intradimer DM interaction which mixes  $S = 1, S^z = 0$  state with  $S = 0$  state and shifts the energy of the  $S = 1, S^z = 0$  up by  $\frac{D^2}{4J_{rung}}$ . However both interdimer and intradimer DM interaction results in the easy-axis anisotropy for the triplet excitations (energy of the  $S^z = \pm 1$  states is lower than the energy of the  $S^z = 0$  state).

Note also, that the effective anisotropy for the triplet excitations is easy axis, while usually anisotropy due to DM interaction (e.g., anisotropy of the order parameter in the ordered state of an antiferromagnet) is of easy plane type. This "inversion" of anisotropy seems to be a common feature of all spin-gap magnets: it was obtained by perturbative analysis of the role of single-ion anisotropy in Haldane magnet<sup>39</sup> and was observed in a Haldane magnet  $\text{PbNi}_2\text{V}_2\text{O}_8$ ,<sup>40</sup> similar inversion of the anisotropy type between the anisotropy of triplet excitations and order parameter anisotropy in a field-induced ordered phase of a spin-gap magnet follows from macroscopic approach<sup>5</sup>.

Effect of the symmetric anisotropic coupling on a strong-rung ladder can be considered similarly. Our aim here is to illustrate that its contribution is linear on coupling parameter along the rung so we consider simple axial SAE coupling in the form

$$V = A_{leg} \sum_{n,j} S_{j,n}^z S_{j,n+1}^z + A_{rung} \sum_n S_{1,n}^z S_{2,n}^z \quad (B6)$$

here  $n$  enumerates rungs (dimers) and  $j$  enumerates legs of the ladder (spins in the dimer),  $A_{leg}$  and  $A_{rung}$  are SAE coupling constants along the leg and rung of the ladder.

By applying this operator to the ground state and to the one-particle excited states one can ascertain that SAE coupling along the legs mixes ground state and single-particle states with two-particle states and will give some corrections in the second order of perturbations, while SAE coupling on the rungs gives energy corrections already in the first order on the coupling parameter: energies of the ground state and of the  $S^z = 0$  component of triplet state are shifted (per dimer) by  $-\frac{1}{4}A_{rung}$ , while energies of the  $S^z = \pm 1$  components are shifted by  $+\frac{1}{4}A_{rung}$ . Zero field splitting of triplet levels appears, its type (easy axis or easy plane) depends on the coupling parameter  $A_{rung}$  sign, which can be both positive and negative.

\* glazkov@kapitza.ras.ru

† Current address: Quantum Device Physics Labora-

tory, Department of Microtechnology and Nanoscience, Chalmers University of Technology SE-412 96 Göteborg,



Sweden

- <sup>‡</sup> Current address: Heinz Maier-Leibnitz Zentrum (MLZ) Garching, D-85748 Germany
- <sup>1</sup> H.J.Mikeska and A.K.Kolezhuk, Lect. Notes Phys., **645**, 1-83 (2004)
  - <sup>2</sup> M. Hagiwara, L. P. Regnault, A. Zheludev, A. Stunault, N. Metoki, T. Suzuki, S. Suga, K. Kakurai, Y. Koike, P. Vorderwisch, and J.-H. Chung, Phys. Rev. Lett. **94**, 177202 (2005)
  - <sup>3</sup> Ian Affleck, Physical Review B **46**, 9002 (1992)
  - <sup>4</sup> A.M. Tsvelik, Physical Review B **42**, 10499 (1990)
  - <sup>5</sup> A.M. Farutin and V.I. Marchenko, Zh.Eksp.Teor.Fiz. **131** 860 (2007) (JETP **104** 751 (2007))
  - <sup>6</sup> A.K. Kolezhuk, V.N. Glazkov, H. Tanaka, and A. Oosawa Physical Review B **70**, 020403 (2004)
  - <sup>7</sup> K. Yu. Povarov, A. I. Smirnov, O. A. Starykh, S. V. Petrov, and A. Ya. Shapiro, Physical Review Letters **107**, 037204 (2011)
  - <sup>8</sup> A. Shapiro, C. P. Landee, M. M. Turnbull, J. Jornet, M. Deumal, J. J. Novoa, M. A. Robb, and W. Lewis, J. Am. Chem. Soc. **129**, 952 (2007)
  - <sup>9</sup> T. Hong, Y. H. Kim, C. Hotta, Y. Takano, G. Tremelling, M. M. Turnbull, C. P. Landee, H.-J. Kang, N. B. Christensen, K. Lefmann, K. P. Schmidt, G. S. Uhrig, and C. Broholm, Phys. Rev. Lett. **105**, 137207 (2010).
  - <sup>10</sup> D. Schmidiger, S. Mühlbauer, S. N. Gvasaliya, T. Yankova, and A. Zheludev Phys. Rev. B **84**, 144421 (2011)
  - <sup>11</sup> D. Schmidiger, P. Bouillot, S. Mühlbauer, S. Gvasaliya, C. Kollath, T. Giamarchi, and A. Zheludev Phys. Rev. Lett. **108**, 167201 (2012)
  - <sup>12</sup> J. L. White, C. Lee, Ö. Günaydin-Şen, L. C. Tung, H. M. Christen, Y. J. Wang, M. M. Turnbull, C. P. Landee, R. D. McDonald, S. A. Crooker, J. Singleton, M.-H. Whangbo, and J. L. Musfeldt Phys. Rev. B **81**, 052407 (2010)
  - <sup>13</sup> R. M. Eremina, M. V. Eremin, V. N. Glazkov, H.-A. Krug von Nidda and A. Loidl, Physical Review B **68**, 014417 (2003)
  - <sup>14</sup> Hitoshi Ohta, Tatsuya Yamasaki, Susumu Okubo, Takahiro Sakurai, Masashi Fujisawa, Hikomitsu Kikuchi, Journal of Physics: Conference Series **320** 012026 (2011)
  - <sup>15</sup> P.W.Anderson, Journal of the Physical Society of Japan **9** (1954), 316
  - <sup>16</sup> L.H.Piette, W.A.Anderson, Journal of Chemical Physics **34** (1959), 899
  - <sup>17</sup> M. A. Fayzullin, R. M. Eremina, M. V. Eremin, A. Dittl, N. van Well, F. Ritter, W. Assmus, J. Deisenhofer, H.-A. Krug von Nidda, and A. Loidl Physical Review B **88**, 174421 (2013)
  - <sup>18</sup> M. Heinrich, H.-A. Krug von Nidda, A. Krimmel, A. Loidl, R. M. Eremina, A. D. Ineev, B. I. Kochelaev, A. V. Prokofiev, and W. Assmus, Physical Review B **67**, 224418 (2003).
  - <sup>19</sup> A. Abragam, B. Bleaney, Electron paramagnetic resonance of transition ions, Clarendon Press, Oxford (1970)
  - <sup>20</sup> S.A.I'tshuler, B.Kozyrev, Electron Paramagnetic Resonance, Academic Press (1964)
  - <sup>21</sup> S.C.Furuya and M.Sato, Journ. Phys. Soc. Japan **84**, 033704 (2015)
  - <sup>22</sup> M. Oshikawa and I. Affleck, Physical Review B **65**, 134410(2002)
  - <sup>23</sup> V.N.Glazkov, A.I. Smirnov, H. Tanaka and A. Oosawa, Physical Review B, **69** 184410 (2004).
  - <sup>24</sup> V. N. Glazkov, T. S. Yankova, J. Sichelschmidt, D. Hüvonen, A. Zheludev, Physical Review B, **85**, 054415 (2012)
  - <sup>25</sup> D.B.Chestnut and W. D. Phillips. Journal of Chemical Physics, **35**, 1002 (1961).
  - <sup>26</sup> P. W. Anderson and P. R. Weiss, Rev. Mod. Phys., **25**, 269 (1953).
  - <sup>27</sup> T. G. Castner, Jr. and Mohidar S. Seehra, Phys. Rev. B, **4**, 38 (1971).
  - <sup>28</sup> J. H. Van Vleck, Phys. Rev., **74**, 1168 (1948).
  - <sup>29</sup> D.V. Zakharov et al., in Quantum Magnetism, edited by B. Barbara et al. (Springer, Dordrecht, 2008).
  - <sup>30</sup> D. L. Huber, G. Alejandro, A. Caneiro, M. T. Causa, F. Prado, M. Tovar Phys. Rev. B, **60**, 12155 (1999)
  - <sup>31</sup> I. Yamada, M. Nishi, J. Akimutsu J. Phys.: Condens. Matter, **8**, 2625 (1996).
  - <sup>32</sup> M.V. Eremin, D.V. Zakharov, H.-A. Krug von Nidda, R.M. Eremina, A. Shuvaev, A. Pimenov, P. Ghigna, J. Deisenhofer and A. Loidl Physical Review Letters, **101**, 147601 (2008).
  - <sup>33</sup> T. Moriya, Phys. Rev., **120**, 91 (1960).
  - <sup>34</sup> A. S. Moskvina and I. G. Bostrem, Sov. Phys. Solid State, **19**, 1532 (1977).
  - <sup>35</sup> F. Keffer, Phys. Rev., **126**, 896 (1962).
  - <sup>36</sup> M. V. Eremin, in Spektroskopiya Kristallov, edited by A. A. Kapliyanski (Nauka, Leningrad, 1965).
  - <sup>37</sup> L.-P. Regnault, I.A. Zaliznyak and S.V. Meshkov J.Phys.:Condens.Matter **5** L677 (1993)
  - <sup>38</sup> A. I. Smirnov, T. A. Soldatov, K. Yu. Povarov, A. Ya. Shapiro, Phys. Rev. B **91**, 174412 (2015)
  - <sup>39</sup> O. Golinelli, Th. Jolicoeur, and R. Lacaze, J. Phys.: Condens. Matter **5**, 7847 (1993)
  - <sup>40</sup> A. I. Smirnov, V. N. Glazkov, T. Kashiwagi, S. Kimura, M. Hagiwara, K. Kindo, A. Ya. Shapiro, and L. N. Demianets, Physical Review B, **77**, 100401(R) (2008)